NeuroImage: Clinical 11 (2016) 124–132

Contents lists available at ScienceDirect

NeuroImage: Clinical

journal homepage: www.elsevier.com/locate/ynicl

Wavelet coherence analysis of dynamic cerebral autoregulation in neonatal hypoxic–ischemic encephalopathy

Fenghua Tian[a], Takashi Tarumi[b,c,d], Hanli Liu[a], Rong Zhang[b,c,d], Lina Chalak[e,*]

[a]Department of Bioengineering, University of Texas at Arlington, United States
[b]Department of Internal Medicine, University of Texas Southwestern Medical Center, United States
[c]Department of Neurology and Neurotherapeutics, University of Texas Southwestern Medical Center, United States
[d]Institute for Exercise and Environmental Medicine, Texas Health Presbyterian Hospital of Dallas, United States
[e]Department of Pediatrics, University of Texas Southwestern Medical Center, United States

ARTICLE INFO

Article history:
Received 24 September 2015
Received in revised form 16 January 2016
Accepted 23 January 2016
Available online 25 January 2016

Keywords:
Hypoxic–ischemic encephalopathy (HIE)
Hypothermia
Cerebral autoregulation
Near infrared spectroscopy (NIRS)
Wavelet coherence

ABSTRACT

Cerebral autoregulation represents the physiological mechanisms that keep brain perfusion relatively constant in the face of changes in blood pressure and thus plays an essential role in normal brain function. This study assessed cerebral autoregulation in nine newborns with moderate-to-severe hypoxic–ischemic encephalopathy (HIE). These neonates received hypothermic therapy during the first 72 h of life while mean arterial pressure (MAP) and cerebral tissue oxygenation saturation ($S_{ct}O_2$) were continuously recorded. Wavelet coherence analysis, which is a time-frequency domain approach, was used to characterize the dynamic relationship between spontaneous oscillations in MAP and $S_{ct}O_2$. Wavelet-based metrics of phase, coherence and gain were derived for quantitative evaluation of cerebral autoregulation. We found cerebral autoregulation in neonates with HIE was time-scale-dependent in nature. Specifically, the spontaneous changes in MAP and $S_{ct}O_2$ had in-phase coherence at time scales of less than 80 min (<0.0002 Hz in frequency), whereas they showed anti-phase coherence at time scales of around 2.5 h (~0.0001 Hz in frequency). Both the in-phase and anti-phase coherence appeared to be related to worse clinical outcomes. These findings suggest the potential clinical use of wavelet coherence analysis to assess dynamic cerebral autoregulation in neonatal HIE during hypothermia.

1. Introduction

Birth asphyxia is a global burden in clinical neonatal care (Levene et al., 1985). Every year four million newborns are affected worldwide, of which one million die and another million are left with disabilities. Hypothermia is a neuroprotective therapy to improve clinical outcomes by reducing body temperature of newborns for a specific duration of time (Shankaran et al., 2005). However, even following the introduction of hypothermic therapy for neonatal hypoxic–ischemic encephalopathy (HIE), approximately 40% of newborns still have neurodevelopmental abnormalities at 24 months of age (Zonta et al., 2003; Bryce et al., 2005; Higgins et al., 2011). A better understanding of pathophysiological mechanisms of HIE-related brain injury is essential for developing new effective interventions to improve clinical outcomes.

The healthy brain is protected by the mechanisms of cerebral autoregulation, which maintains cerebral blood flow (CBF) at a relatively constant rate across a wide range of arterial blood pressures. In asphyxiated newborns, invasive positron emission tomography (PET) studies reported impairment of cerebral autoregulation with associated vasoparalysis (Pryds et al., 1990). However, it remains unknown whether hypothermic therapy in asphyxiated newborns alters cerebral autoregulation. In addition, there is a lack of methodology that can quantify cerebral autoregulation non-invasively and reliably at the bedside.

In the last decade, significant progress has been made in developing methods to assess cerebral autoregulation based on spontaneous oscillations in blood pressure, CBF, and cerebral oxygenation (Panerai, 1998). Both CBF and cerebral oxygenation can be measured with non-invasive techniques. Specifically, blood flow velocity in the basal cerebral arteries can be measured using transcranial Doppler (TCD) ultrasonography (Aaslid et al., 1982), and cerebral oxygenation can be measured with near-infrared spectroscopy (NIRS) represented as either the difference between the oxygenated and deoxygenated hemoglobin (HbD = HbO_2 − Hb) (Tsuji et al., 2000; Soul et al., 2007; Govindan et al., 2014) or cerebral tissue oxygen saturation ($S_{ct}O_2$) (Caicedo et al., 2011a; Caicedo et al., 2011b; Gilmore et al., 2011; Wong et al., 2012). Both variables are reliable surrogates for changes in CBF as demonstrated in animal models (Tsuji et al., 1998; Brady et al., 2007; Brady et al., 2008; Hahn et al., 2011; Lee et al., 2011; Lee et al., 2012). In particular, $S_{ct}O_2$ is less prone to the movement artifacts during continuous, long-term measurements as compared with HbD (van Bel et al., 2008; Caicedo et al., 2011a).

* Corresponding author at: Pediatrics, University of Texas Southwestern Medical Center, 5323 Harry Hines Blvd. (Room F3.312B), Dallas, TX 75390-9063, United States.
E-mail address: Lina.chalak@utsouthwestern.edu (L. Chalak).

http://dx.doi.org/10.1016/j.nicl.2016.01.020

To assess cerebral autoregulation in the face of dynamic changes in blood pressure, referred to as dynamic cerebral autoregulation, transfer function (Zhang et al., 1998) and other analysis methods for dynamic systems have been developed (Liu et al., 2015). These methods are often based on an assumption that changes in blood pressure and cerebral hemodynamics are stationary, that is, assuming the statistical properties of these variables do not change with time. In reality, blood pressure and cerebral hemodynamics are non-stationary in nature, particularly under pathophysiological conditions (Panerai, 2014). Hence, better tools are needed to characterize the non-stationary aspects of cerebral autoregulation.

Continuous wavelet transform (CWT) is a powerful mathematical tool for time-frequency domain analysis of stationary and non-stationary time series (Torrence and Compo, 1998; Mallat, 1999). Wavelet coherence analysis, based on CWT, characterizes intermittent cross-correlations between two time series at multiple time scales (Grinsted et al., 2004), which makes no assumption about the stationarity of input signals. In this study, we introduced wavelet coherence analysis to assess dynamic cerebral autoregulation in newborns with HIE. All hemodynamic data, including mean arterial pressure (MAP) and $S_{ct}O_2$, were recorded continuously during the first 72 h of life under hypothermic therapy. Wavelet coherence analysis was performed to quantify the spectral power and the dynamic relationship between spontaneous oscillations in MAP and $S_{ct}O_2$. Wavelet-based metrics of phase, coherence and gain were derived for quantitative evaluation of cerebral autoregulation. Potential prognostic values of these metrics for clinical magnetic resonance imaging (MRI) and neurodevelopmental outcomes were explored to reveal short- and long-term neurologic complications in HIE patients.

2. Materials and methods

2.1. Subjects, clinical care and outcome evaluations

This study included newborn infants at ≥36 weeks of gestation with a birth weight of ≥1800 g who were admitted to the neonatal intensive care unit at Parkland Hospital, Dallas, TX, from January 2011 to January 2012. These newborns had perinatal asphyxia or metabolic acidosis, including a clinical symptom of moderate to severe encephalopathy within the first six hours of birth. The study was approved by the Institutional Review Board of the University of Texas Southwestern Medical Center and informed consent was obtained from parents before enrollment.

Perinatal acidemia was determined by blood gases measured from umbilical arterial blood during delivery. The criteria included a pH of 7.0 or less, a base deficit of 16 mEq/L or greater in umbilical artery blood, or any postnatal blood sample within one hour of life. In order to establish the diagnosis of encephalopathy, a neurological examination was performed within six hours of birth according to the National Institute of Child Health and Human Development (NICHD) classification for modified Sarnat staging (Sarnat and Sarnat, 1976), which assessed 1) level of consciousness, 2) spontaneous activity, 3) posture, 4) tone, 5) primitive reflexes, and 6) autonomic nervous system. Newborns that were diagnosed with moderate or severe encephalopathy for at least three of the six categories were abnormal and would receive hypothermic therapy (Shankaran et al., 2005). Whole-body hypothermia was initiated within six hours after birth and achieved by placing the newborns on a cooling blanket (Blanketrol II, Cincinnati Sub-Zero). The esophageal temperature was maintained at 33.5 °C by the blanket servomechanism for 72 h. Then whole-body rewarming was initiated by increasing the temperature of the blanket by 0.5 °C per hour using the previously published protocols (Shankaran et al., 2005).

Clinical outcome of the hypothermic therapy was evaluated in two stages: First, 3-Tesla MRI (Philips Healthcare Systems, TX) was performed on each HIE survivor within 5–8 days of age for evidence of neurological abnormalities and injuries. MRI findings were scored for abnormalities by an experienced pediatric neuro-radiologist based on the NICHD summary classification, which has been validated in this population to predict outcomes following hypothermia (Chalak et al., 2014b; Rollins et al., 2014). Second, outpatient neurodevelopmental follow-ups were performed at 18 to 24 months of age using the previously published protocol (Chalak et al., 2014a). Bayley-III scales of neurodevelopment were rated in three domains: cognitive, language and motor. Neurodevelopmental delay was identified by at least one Bayley-III scale <85 or cerebral palsy.

2.2. Blood pressure and NIRS monitoring

Intra-arterial blood pressure was continuously measured from an indwelling umbilical arterial catheter. Regional $S_{ct}O_2$ was measured on the frontoparietal side of the neonate's head using an INVOS™ 4100–5100 oximetry (Somanetics, Troy, MI) and a neonatal sensor. Both MAP and $S_{ct}O_2$ data were sampled at a rate of two data points per minute and recorded synchronously with a Vital Sync™ system (Somanetics Corporation, Troy, Michigan).

The MAP and $S_{ct}O_2$ data were collected only under clinically stable conditions (pCO_2 between 40 to 50 mm Hg and hemoglobin level between 12 to 15 mg/dl). Therefore, the actual length of recorded data was less than 72 h and varied case by case. Neonates were selected only if they did not require any vasopressor medications, to avoid potential drug effects on cerebral autoregulation.

2.3. Data preprocessing

Both the MAP and $S_{ct}O_2$ data were first inspected to identify artifacts that were defined as a sharp change of signals greater than 15% from the baseline. These spikes were removed by linear interpolation. Then a second-order polynomial detrending was applied to remove the slow drifts from each time series.

2.4. Wavelet coherence analysis

Wavelet coherence analysis is based on CWT, which decomposes a time series in time-frequency domain by successively convolving the time series with the scaled and translated versions of a mother wavelet function ψ_0 (Mallat, 1999). The continuous wavelet transform of a time series $x(n)$ of length N, which is sampled from a continuous signal at a time step of Δt, is defined as:

$$W^X(n,s) = \sqrt{\frac{\Delta t}{s}} \sum_{n'-n}^{N} x(n)_0^* \left[(n'-n) \left(\frac{\Delta t}{s} \right) \right] \quad (1)$$

where n is a time index, s denotes the time scale that is in inverse proportion to frequency, and * indicates the complex conjugate.

In analogy to Fourier analysis, a wavelet power spectrum of $x(n)$ can be defined as the wavelet transformation of its autocorrelation function, which is implemented as follows:

$$W^{XX}(n,s) = W^X(n,s) W^{X^*}(n,s). \quad (2)$$

The auto-wavelet power spectrum $W^{XX}(n,s)$ is a real function, which describes the power of $x(n)$ in the time-frequency domain.

Similarly, the cross-wavelet transform of two time series, $x(n)$ and $y(n)$, is defined as:

$$W^{XX}(n,s) = W^X(n,s) W^{Y^*}(n,s). \quad (3)$$

The modulus $|W^{XY}(n,s)|$ represents the amount of joint power between $x(n)$ and $y(n)$, and the complex argument $\Delta\varphi(n,s) = \tan^{-1}\left\{\frac{Im[W^{XY}(n,s)]}{Re[W^{XY}(n,s)]}\right\}$ represents the relative phase between $x(n)$ and $y(n)$.

Similar to the transfer function based on Fourier transform (Zhang et al., 1998), a wavelet transfer function can be defined as:

$$H(n,s) = \frac{S\left[S^{-1}W^{XY}(n,s)\right]}{S\left[S^{-1}W^{XX}(n,s)\right]} \quad (4)$$

where S is a smoothing operator in the time-frequency (scale) domain. The smoothing process is necessary to remove the singularities in wavelet power spectra of $x(n)$ to improve the reliability of $H(n,s)$ estimation (Torrence and Compo, 1998). It can be done using a weighted running average in both the time and scale directions, as given by Torrence and Webster (1999). The modulus of wavelet transfer function, $|H(n, s)|$, represents the relative amplitude (gain) between $x(n)$ and $y(n)$. The complex argument of wavelet transfer function represents the phase relationship between $x(n)$ and $y(n)$.

Similar to the magnitude-squared coherence (MSC) function based on Fourier transform (Zhang et al., 1998), a squared cross-wavelet coherence $R^2(n, s)$ is defined as (Torrence and Webster, 1999):

$$R^2(n,s) = \frac{\left|S\left[S^{-1}W^{XY}(n,s)\right]\right|^2}{S\left[S^{-1}\left|W^{X}(n,s)\right|^2 \cdot SS^{-1}\left|W^{Y}(n,s)\right|^2\right]} \quad (5)$$

where $R^2(n, s)$ ranges between 0 and 1 and can be conceptualized as a localized correlation coefficient between $x(n)$ and $y(n)$ in the time-frequency domain. The statistical significance level of $R^2(n,s)$ can be estimated based on a Monte Carlo simulation of a stochastic Gaussian process (Maraun and Kurths, 2004). Briefly, a large ensemble of surrogate data pairs ($n = 1000$) can be generated with bootstrapping (Efron and Tibshirani, 1993), which has the same coefficients as the real input data pair based on the first-order autoregressive (AR1) model (Grinsted et al., 2004). Then wavelet coherence is calculated for all of the simulated data pairs. The significance level of coherence of the real input data pair is determined by comparing with the statistical distribution of those obtained from the surrogate data pairs at each time and wavelet scale.

In this study, we used a MATLAB-based software package (Grinsted et al., 2004) for wavelet coherence analysis between the spontaneous oscillations of MAP and $S_{ct}O_2$ (MAP → $S_{ct}O_2$). This software package employs a Morlet wavelet (with $\Omega_0 = 6$) as the mother wavelet ψ_0, which provides a good trade-off between time and frequency localization (Grinsted et al., 2004). We confirmed that both the MAP and $S_{ct}O_2$ changes as input data were normally distributed, and their Fourier power spectra could be approximated by the AR1 models in this software package. A 95% confidence interval ($p < 0.05$) was used for statistical testing of the estimated wavelet coherence. A comparison between the results from wavelet coherence analysis and transfer function analysis based on two simulated, stationary time series is given in Supplementary material I.

2.5. Quantifying results from wavelet coherence analysis

To quantitatively evaluate the status of cerebral autoregulation based on wavelet analysis, we first defined four phase ranges: 1) $\Delta\varphi = 0 \pm \pi/4$, 2) $\pi/2 \pm \pi/4$, 3) $\pi \pm \pi/4$, and 4) $-\pi/2 \pm \pi/4$ to characterize the relationship between the changes in MAP and $S_{ct}O_2$. Each phase represented a distinct pattern of coherence and might be related to different underlying mechanisms: $\Delta\varphi = 0 \pm \pi/4$ represented an in-phase coherence where the MAP and $S_{ct}O_2$ oscillated in same directions, $\Delta\varphi = \pi \pm \pi/4$ represented an anti-phase coherence where the MAP and $S_{ct}O_2$ oscillated in opposite directions, $\Delta\varphi = \pi/2 \pm \pi/4$ and $-\pi/2 \pm \pi/4$ represented where the MAP and $S_{ct}O_2$ oscillated with significant phase differences. Therefore, it was important to quantify these patterns separately. Within each phase range, we further defined and quantified two wavelet-derived metrics, namely, percentage of significant coherence $P(s)$ and wavelet transfer function gain $G(s)$, as follows:

1) The percentage of significant coherence $P(s)$ was calculated at each wavelet time scale as the percentage of time during which the squared cross-wavelet coherence R^2 was significantly different from the simulated Gaussian process ($p < 0.05$). $P(s)$ was scale-dependent, as shown in Fig. 1(c). It reflected the overall degree at which the MAP and $S_{ct}O_2$ were correlated at each time scale. Further, for a specific range of time scale, a cross-scale mean value P_{mean} was determined for each of the four phase ranges.
2) The wavelet transfer function gain $G(s)$ was calculated as the mean value of gain at each time scale over the periods where R^2 was statistically significant ($p < 0.05$). $G(s)$ was also scale-dependent. For a specific range of time scale, a cross-scale mean value G_{mean} was determined within the periods of significant coherence for each of the four phase ranges.

In addition, both $P(s)$ and $G(s)$ were calculated outside the cone of influence (COI) to avoid any edge effect.

2.6. Classification and cross-validation

In order to explore the possibility of using wavelet-derived metrics as early predictors for clinical outcomes, we utilized a linear support vector machine (SVM) classifier (Cristianini and Shawe-Taylor, 2000) with leave-one-out cross-validation (LOOCV) (Hjorth, 1994). SVM is a commonly used algorithm in machine learning for pattern recognition and data classification, while LOOCV is a special case of leave-k-out cross validation when k is equal to one (Shao, 1993). In LOOCV, one observation is left out as a test set while the remaining observations are used as a training set to construct a classification model. Then, the model-building and validation process continues until every observation has served as a test set once through the entire data space. The LOOCV analysis utilizes the available data most efficiently since only one observation is left out at each step. Therefore, it has been widely used in studies with small sample sizes (Georgakoudi et al., 2001; Volynskaya et al., 2008; Tian et al., 2009; Derosiere et al., 2014).

In this study, the wavelet-derived metrics (P_{mean} and G_{mean} in four different phase ranges, as described in Section 2.5) from each neonate afforded eight maximal features that could be used to construct the SVM classifier for predicting "normal outcome" or "abnormal outcome" and be cross-validated by LOOCV. Specifically, at each step, one neonate's data was selected as a test set and the remaining eight neonates' data were used as a training set for constructing the classifier. This process was repeated nine times to complete the LOOCV analysis. At last, the classification accuracy across all patients was determined by the percentage of correctly classified patients over the total.

3. Results

Twenty newborns with a gestational age of 39 ± 2 weeks received whole-body hypothermic therapy for 72 h for moderate ($n = 17$) and severe encephalopathy ($n = 3$) during the study period. They all had evidence of multiple organ involvement. Exclusions were done according to the predefined criteria: clinical instability with hypoxia and pulmonary hypertension ($n = 3$), $S_{ct}O_2$ continually exceeding upper limit of 95% for more than 4–6 h ($n = 4$), lack of continuous recording ($n = 3$), and no consent ($n = 1$). Thus, nine neonates (moderate/severe = 7/2) had complete monitoring data and were analyzed in this report. Among these nine neonates, one died after extracorporeal membrane oxygenation (ECMO) following hypothermia; four had abnormal MRIs with evidence of diffuse white matter injury and watershed infarcts and/or neurodevelopmental delays with at least one Bayley III scale <85; the remaining four had normal outcomes. Individual characteristics and clinical outcomes of these neonates are summarized in Table 1.

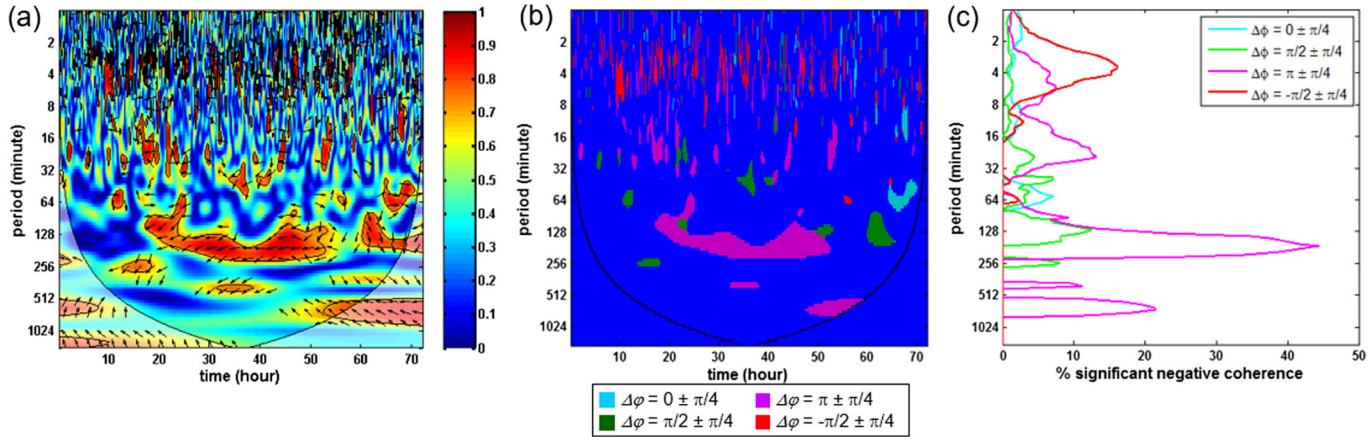

Fig. 1. Quantification of results in wavelet coherence analysis: (a) Squared cross-wavelet coherence, $R_{MAP \rightarrow StcO_2}{}^2(n,s)$, from a HIE neonate. The x-axis represents time, the y-axis represents scale (which has been converted to the equivalent Fourier period), and the color scale represents the magnitude of R^2. The cone of influence (COI) where edge effects should be considered is shown as a lighter shade. The black line contours designate areas of significant coherence ($p < 0.05$). The arrows designate the relative phase between MAP and $S_{ct}O_2$: a rightward-pointing arrow indicates in-phase coherence between the two signals ($\Delta\varphi = 0$), a leftward-pointing arrow indicates anti-phase coherence ($\Delta\varphi = \pi$). (b) Regions of significant coherence ($p < 0.05$) are classified into four phase ranges: $\Delta\varphi = 0 \pm \pi/4$ (cyan), $\pi/2 \pm \pi/4$ (green), $\pi \pm \pi/4$ (purple), and $-\pi/2 \pm \pi/4$ (red). Regions of non-significant coherence and/or with edge effect appear as blue background. (c) Percentage of significant coherence, $P(s)$, is quantified in each of the four phase ranges. $P(s)$ was a function of scale, which is plotted on the y axis (that has been converted to equivalent Fourier period). At each scale, $P(s)$ was calculated as the percentage of time during which the R^2 was statistically significant ($p < 0.05$). (For interpretation of the references to color in this figure legend, the reader is referred to the web version of this article.)

Because the MAP and $S_{ct}O_2$ data were collected when patients were clinically stable, artifacts were only detected at a number of isolated time points. Thus, wavelet analysis was conducted on the complete, continuous data from each patient after removing the artificial spikes. The results of wavelet coherence from all of the nine individual neonates are given in Supplementary material II.

3.1. Characteristics of phase, coherence and gain between MAP and $S_{ct}O_2$ oscillations

All of the neonates with normal clinical outcomes showed non-significant MAP → $S_{ct}O_2$ coherence most of the time during hypothermia, indicating that the spontaneous oscillations of $S_{ct}O_2$ were largely irrelevant to the systemic changes in blood pressure. In contrast, significant MAP → $S_{ct}O_2$ coherence was observed among the neonates with abnormal outcomes, which was often sustained for hours to days and in different ranges of the wavelet time scale. Two individual examples are detailed below:

Fig. 2(a) shows the MAP → $S_{ct}O_2$ coherence from a neonate who received whole-body hypothermia for moderate encephalopathy (Patient #7). Intermittent in-phase coherence between the MAP and $S_{ct}O_2$ changes was observed in a scale range of 8 to 64 min. This phenomenon was further confirmed in a segment of real-time data shown in Fig. 2(b). In addition, Fig. 2(a) also shows a transient, anti-phase MAP → $S_{ct}O_2$ coherence at the early stage of hypothermia that locates in a longer scale range of 256 to 512 min. The significant, intermittent in-phase coherence between the MAP and $S_{ct}O_2$ changes indicated that the patient's cerebral oxygenation was passive to the blood pressure changes during hypothermia, a vital sign of an impaired autoregulation system (Soul et al., 2007). Following the treatment, the neonate was transferred to ECMO because of severe pulmonary hypertension and subsequently died after withdrawal of care.

Fig. 2(c) shows the MAP → $S_{ct}O_2$ coherence from a neonate who was treated for severe encephalopathy (Patient #5). A predominant anti-phase coherence between the MAP and $S_{ct}O_2$ oscillations was observed in a scale range of 64 to 256 min. This phenomenon was further confirmed in a segment of real-time data shown in Fig. 2(d), in which both MAP and $S_{ct}O_2$ oscillated at a periodicity of around 2 h and in a clear anti-phase relationship. Post-treatment evaluations showed the patient had both abnormal MRIs prior to hospital discharge and severe neurodevelopmental delays at 2 years of age (all of the Bayley III scales were <85).

At group level, the significant in-phase and anti-phase MAP → $S_{ct}O_2$ coherence among the patients with abnormal outcomes were scale-dependent (Fig. 3). The in-phase MAP → $S_{ct}O_2$ coherence was represented mostly in a shorter scale range below 80 min with a peak around 7.5 min. In contrast, the significant anti-phase MAP → $S_{ct}O_2$ coherence was represented in a much broader scale range with a peak at about 2.5 h.

Neither the normal-outcome group nor the abnormal-outcome group had significant MAP → $S_{ct}O_2$ coherence in the other two phase ranges, namely $\Delta\varphi = \pi/2 \pm \pi/4$ and $-\pi/2 \pm \pi/4$. These two phase ranges seemed irrelevant to the status of cerebral autoregulation. Therefore, the results from these two phase ranges were not utilized in the analysis hereafter.

Further quantification of results was conducted in a predefined scale range of 7.5 min to 5 h. Here the upper bound was selected because of

Table 1
Individual characteristics and clinical outcomes of the nine neonates reported in this study.

Patient #	Gender	Gestation age (week)	Encephalopathy	MRI	Bayley-III (cognitive/language/motor)
1	F	40	Moderate	Normal	50/75/89
2*	M	39	Severe	Normal	100/90/85
3	M	42	Moderate	Normal	77/75/94
4	M	37	Moderate	Normal	70/68/91
5	F	38	Severe	Abnormal	55/74/82
6*	F	36	Moderate	Normal	90/91/85
7	M	40	Moderate	Death	Death
8*	F	38	Moderate	Normal	85/91/94
9*	M	36	Moderate	Normal	85/97/88

* Neonates with normal clinical outcomes.

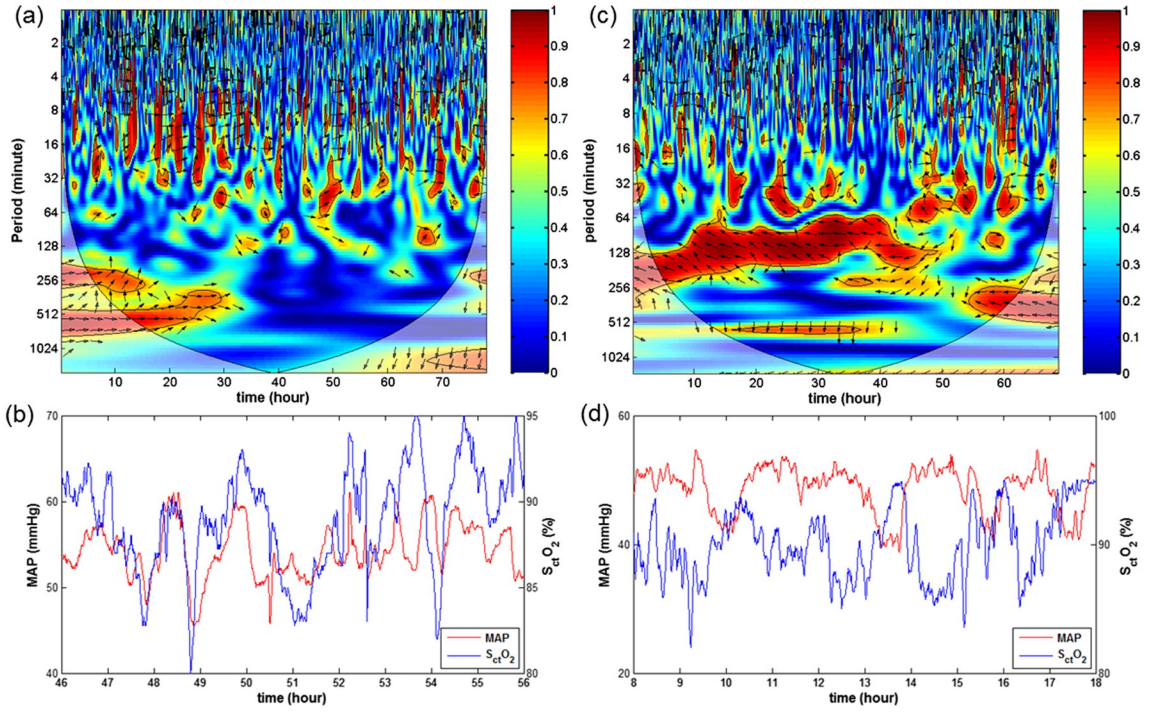

Fig. 2. Wavelet-based MAP → $S_{ct}O_2$ coherence in two neonates with abnormal outcomes: (a) In this squared cross-wavelet coherence, $R_{MAP \to SctO_2}{}^2(n,s)$, from the first neonate who was treated for moderate encephalopathy, the x-axis represents time, the y-axis represents scale (which has been converted to equivalent Fourier period), and the color scale represents the magnitude of R^2. The cone of influence (COI) where edge effects should be considered is shown as a lighter shade. The black line contours designate areas of significant coherence ($p < 0.05$). The arrows designate the relative phase between MAP and $S_{ct}O_2$: a rightward-pointing arrow indicates in-phase coherence between the two signals ($\Delta\varphi = 0$), a leftward-pointing arrow indicates anti-phase coherence ($\Delta\varphi = \pi$). (b) An enlarged segment of the real-time MAP and $S_{ct}O_2$ data from the first neonate. The two signals fluctuate synchronously in a clear in-phase relationship. (c) Squared cross-wavelet coherence, $R_{MAP \to SctO_2}{}^2(n,s)$, is shown from the second neonate who was treated for severe encephalopathy. (d) An enlarged segment of the real-time MAP and $S_{ct}O_2$ data is shown from the second neonate. The two signals fluctuate in a clear anti-phase relationship with a periodicity of around 2 h. (For interpretation of the references to color in this figure legend, the reader is referred to the web version of this article.)

the significant edge effect of CWT in time scales longer than 5 h; and the lower bound was selected to constrain the influence of transient noises. The group-averaged mean percentage of significant coherence, P_{mean}, and the associated mean gain, G_{mean}, were calculated within the predefined scale range. Overall, patients with abnormal outcomes showed either a greater in-phase P_{mean} ($p = 0.15$, two-sample t-test) or a greater anti-phase P_{mean} ($p = 0.27$, two-sample t-test) than the patients with normal outcomes as shown in Fig 4 (a). The abnormal-outcome group also showed either a higher in-phase G_{mean} ($p = 0.03$, two-sample t-test) or a higher anti-phase G_{mean} ($p = 0.39$, two-sample t-test) than the normal-outcome group as shown in Fig 4(b).

3.2. Predictive accuracy of clinical outcomes based on the wavelet-derived metrics

Table 2 summarizes the accuracy of wavelet-derived metrics in predicting the patients' clinical outcomes, which was estimated by the LOOCV analysis with linear SVM classifiers. The predictive accuracy varied from 66.7% to 88.9% based on the use of different combinations of

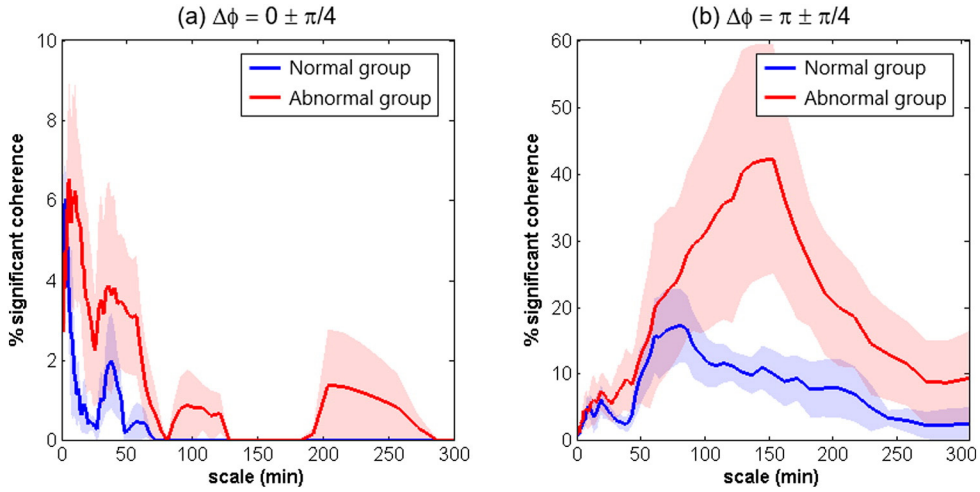

Fig. 3. Scale-dependent percentage of significant MAP → $S_{ct}O_2$ coherence, $P(s)$, quantified in two phase ranges: (a) $\Delta\varphi = 0 \pm \pi/4$, and (b) $\Delta\varphi = \pi \pm \pi/4$. In each graph, the solid lines denote the group-averaged values and the shaded regions denote the standard errors.

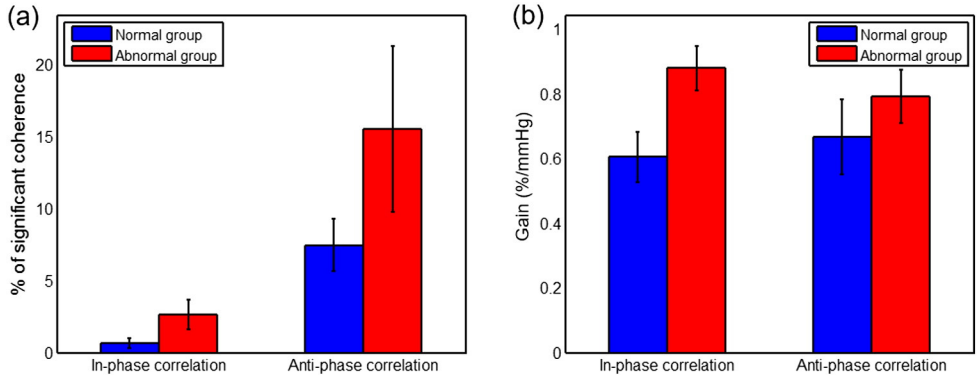

Fig. 4. Wavelet coherence and gain estimation at group level: (a) mean percentage of the significant coherence, P_{mean}, over the time scales of 7.5 min to 5 h, and (b) mean gain associated with the significant coherence, G_{mean}. In each graph, the data are plotted as mean ± standard error.

wavelet-derived metrics. The best accuracy was achieved when all of the in-phase and anti-phase measures of phase and gain were utilized.

4. Discussion

The current study assessed cerebral autoregulation in neonates with HIE by employing a novel wavelet coherence analysis to characterize the dynamic relationship between the spontaneous MAP and $S_{ct}O_2$ oscillations, while the neonates were receiving hypothermic therapy during the first 72 h of life. The wavelet-derived metrics of phase, coherence and gain for quantitative evaluation of cerebral autoregulation indicate a potential to use this methodology to predict clinical outcomes during early phase of neonatal care at the bedside.

Asphyxia starts with a fetal insult due to ischemic attack that impairs CBF regulation as a consequence of a substantial interruption of maternal and/or fetal placental blood flow and gas exchange (Shalak and Perlman, 2004). The timing, severity, pattern and duration of the fetal insults as well as the degree of recovery via fetal compensatory and/or adaptive mechanisms determine the spectrum of disease, outcomes and possibly the responses to therapy. While hypothermic therapy provides neuroprotection via multiple pathways, including the reduction in cerebral metabolism as well as CBF (Laptook et al., 1999; Laptook et al., 2001; Laptook, 2009), a significant knowledge gap exists regarding how to viably assess cerebrovascular functions in general, and cerebral autoregulation in particular, during the treatment and more importantly, how potential impairment in cerebral autoregulation may be related to the clinical outcomes.

Previous studies evaluating cerebral autoregulation in newborns have utilized technically challenging imaging modalities for CBF measurement such as PET, single photon emission computed tomography (SPECT), or perfusion-weighted MRI. Other more recent studies have recognized the utility of non-invasive NIRS measurements (Greisen, 2006), and have linked high cerebral oxygen saturation, a pattern indicative of irreversible brain injury, to the death and poor neurodevelopmental outcomes in HIE patients (Meek et al., 1999; Toet et al., 2006; Ancora et al., 2013; Lemmers et al., 2013). Autoregulation in preterm newborns has been extensively and elegantly studied non-invasively by quantifying the coherence over short time scales using NIRS-derived HbD and $S_{ct}O_2$ (Tsuji et al., 2000; Soul et al., 2007; Govindan et al., 2014). In the present study, we chose to use $S_{ct}O_2$ rather than HbD as an index of cerebral blood flow dynamics, as the former is less sensitive to movement artifact (van Bel et al., 2008; Caicedo et al., 2011a) and therefore more suitable for the purpose of long time scale recording. Moreover, $S_{ct}O_2$ has been validated to correlate well with MRI arterial spin label cerebral blood flow in the setting of HIE (Wintermark et al., 2014).

Possible confounders involve the properties of $S_{ct}O_2$ which can be affected by arterial saturation, CBF, cerebral blood volume and cerebral oxygen consumption (van Bel et al., 2008; Chalak et al., 2014c). Therefore, these variables need to be stable in order for $S_{ct}O_2$ to reflect accurate steady-state measurements of CBF (Shalak and Perlman, 2004). We attempted to control for this by including data collected under clinically stable conditions and normative parameters for dextrose and hemoglobin. We focused on early recognition of autoregulatory impairments in newborns with HIE by interrogating the relationship between spontaneous changes in MAP and $S_{ct}O_2$ measured at the bedside. Such neonates with limited responses to hypothermia, if recognized early, might benefit from new or additional neuroprotective therapies if they become available.

Transfer function analysis has been widely used to assess dynamic cerebral autoregulation in preterm newborns (Tsuji et al., 2000; Soul et al., 2007). These studies reported a pressure-passive status of impaired cerebral autoregulation as indicated by an in-phase coherence between the spontaneous MAP and $S_{ct}O_2$ changes. An intrinsic limitation of transfer function analysis is that it is based on an assumption that the changes in MAP and $S_{ct}O_2$ are stationary, which may not always hold in clinical settings such as HIE. Indeed, our data analysis indicates that transfer function metrics represent the averaged data of phase, coherence and gain in the frequency domain and are unable to characterize the intermittent coherence between two signals (see Supplementary material III). Alternatively, several studies used a moving window correlation method that estimated time-varying correlation coefficients between the spontaneous changes in MAP and $S_{ct}O_2$ (Gilmore et al., 2011). The size of moving window was typically set at 30 min (Gilmore et al., 2011), which limited its capacity to assess cerebral autoregulation over multiple time scales.

Assessment of dynamic cerebral autoregulation using wavelet coherence makes no assumption about the stationarity of input signals. A study by Latka et al. (2005) demonstrated that the phase dynamics between the spontaneous changes in MAP and CBF velocity measured in the middle cerebral artery (MCA), which was based on wavelet analysis, accounted for most of the nonlinear and non-stationary properties of cerebral autoregulation. Another study by Rowley et al. (2007) showed that the wavelet-based coherence was useful for evaluating dynamic properties of cerebral autoregulation in autonomic failure patients in response to a short-duration posture change. In this study, we applied wavelet coherence analysis to assess dynamic cerebral autoregulation in neonates with HIE at multiple time scales, which were the intrinsic characteristics of the continuously recorded MAP and $S_{ct}O_2$ changes for up to 72 h. Wavelet-based metrics of phase, coherence,

Table 2
Accuracy of wavelet-derived metrics in predicting the patients' clinical outcomes.

Parameters	Predictive accuracy
In-phase P_{mean}, anti-phase P_{mean}	77.8%
In-phase G_{mean}, anti-phase G_{mean}	66.7%
In-phase P_{mean} & G_{mean}, anti-phase P_{mean} & G_{mean}	88.9%

and gain were derived to quantify the severity of impaired cerebral autoregulation. Preliminary findings suggest that these measures appear to be useful for predicting the short-term and long-term clinical outcomes following hypothermic therapy.

In wavelet coherence analysis, statistical significance of coherence between the MAP and $S_{ct}O_2$ changes was estimated using a Monte Carlo simulation method, which generated a large ensemble of surrogate data pairs based on bootstrapping and an AR1 model. We confirmed that the estimated Fourier power spectra of MAP and $S_{ct}O_2$ changes could be approximated by the AR1 model, which supports the use of this method for statistical testing (Grinsted et al., 2004).

The main findings of this study indicate that cerebral autoregulation in neonates with HIE is a time-scale-dependent phenomenon: Significant in-phase coherence between the MAP and $S_{ct}O_2$ oscillations occurred mostly in shorter time scales of $\leq$80 min with a peak of around 7.5 min, and significant anti-phase coherence between these two oscillations occurred in longer time scales of around 2.5 h. Both appeared to be related to worse clinical outcomes. Our finding of the in-phase coherence between MAP and $S_{ct}O_2$ is in line with the previous findings of a pressure-passive status of impaired cerebral autoregulation that corresponded to changes occurring over several minutes (Tsuji et al., 2000; Soul et al., 2007; Gilmore et al., 2011). However, our finding of persistent anti-phase coherence between MAP and $S_{ct}O_2$ oscillations at a large time scale of about 2.5 h was unexpected. Currently, there are no comparisons available at these large time scales from the literature. The anti-phase coherence between MAP and $S_{ct}O_2$ may have different underlying pathophysiological mechanisms from those of the pressure-passive status of impaired cerebral autoregulation, which need to be elucidated in further studies. As discussed above, possible confounders involve the properties of $S_{ct}O_2$ which can be affected by arterial saturation, CBF, cerebral blood volume and cerebral oxygen consumption (van Bel et al., 2008; Chalak et al., 2014c). Therefore, these variables need to be stable in order for $S_{ct}O_2$ to reflect accurate steady-state measurements of CBF (Shalak and Perlman, 2004). We attempted to control for this by including data collected under clinically stable conditions and normative parameters for dextrose and hemoglobin. The newborns selected had stable cardiovascular variables with respect to arterial oxygenation and ventilation, and body temperatures were maintained constant at 33.5 °C for the duration of hypothermia. Cerebral hyperoxygenation, abnormally increased perfusion, and lack of normal cerebral blood flow regulation are typically present in severe hypoxic–ischemic encephalopathy and are associated with poor neurodevelopmental outcome (Toet et al., 2006), even when hypothermia is used (Lemmers et al., 2013). Such newborns were excluded from study selection requiring stable hemodynamic measures, which resulted in a less severely affected group, where adaptive mechanisms could also be at play. For instance, with the time scale of 2 h, it is possible that even though brain perfusion might be affected by reductions in arterial pressure, redistribution of oxygenated blood related to the reductions in brain perfusion and neuronal metabolism could lead to an increase in $S_{ct}O_2$. Another possible explanation may rely on the characteristics of spontaneous MAP and $S_{ct}O_2$ oscillations in the power spectra. Fig. 5 shows the estimated Fourier power spectra of the normalized MAP and $S_{ct}O_2$ oscillations for all the neonates based on Welch's method (Welch, 1967). Distinct peaks in MAP are seen in time scales of 80 to 200 min, especially for neonates with abnormal outcomes, which are echoed by the $S_{ct}O_2$ data. Thus, it is possible that the long-term, anti-phase coherence between MAP and $S_{ct}O_2$ reflects a deleterious effect of large blood pressure variability on brain oxygenation homeostasis in newborns with HIE.

This study has several limitations. First, the current data were collected from a small sample of neonates ($n = 9$), which limited the ability to address moderate and severe encephalopathy separately. The findings in the study need to be replicated in larger groups of patients. Second, the data was sampled at two data points per minute as limited by the available hardware for data collection during this study. According to the Nyquist theorem, it only allowed a detection of frequencies up to 0.017 Hz. The relationship between MAP and $S_{ct}O_2$ changes in the very low frequency range and higher ($\geq$0.02 Hz), as defined by previous studies (Zhang et al., 2002), could not be explored. Third, although $S_{ct}O_2$ has been widely used as a surrogate for CBF, in reality it represents a composite result of blood oxygenation from the regional arterioles, capillary vascular beds and post-capillary venues interrogated by NIRS. Redistribution of oxygenated blood among these blood vessels could affect the $S_{ct}O_2$ readings. Additional techniques for direct spot checks measures of CBF, such as TCD (Aaslid et al., 1982) or diffuse correlation spectroscopy (DCS) (Roche-Labarbe et al., 2010; Durduran and Yodh, 2014) could be considered in future studies to complement the continuous $S_{ct}O_2$ measurements. A major limitation of both new techniques to be taken into account is the lack of ability to provide continuous measurements over the long time scales of interest. Moreover, DCS is not readily available outside of a few research centers. Also elegant studies (Volpe, 1981; Greisen, 2006, 2009) in the past few decades have described the limitations of Doppler CBF velocity as a proxy of CBF when an arterial cross sectional area is dynamically regulated.

5. Conclusions

Wavelet coherence analysis is a suitable and powerful tool to characterize and quantify the dynamic status of cerebral autoregulation during

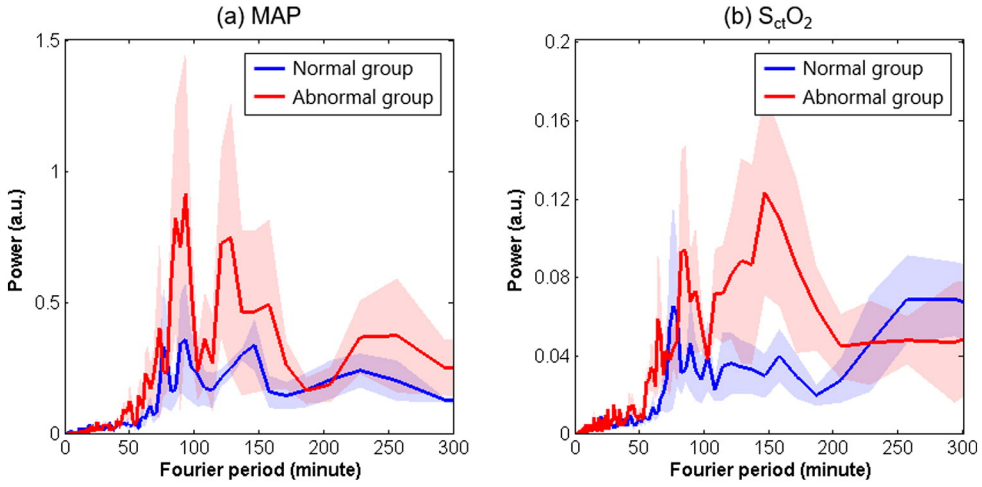

Fig. 5. Estimated Fourier power spectrum density (PSD) of (a) spontaneous MAP oscillations, and (b) spontaneous $S_{ct}O_2$ oscillations in HIE neonates during hypothermia. PSD was estimated based on the normalized MAP and $S_{ct}O_2$ time series (the original time series divided by their mean values) and, therefore, had an arbitrary unit (a.u.).

a long-lasting treatment such as hypothermia. Based on this method, significant in-phase and anti-phase coherence between spontaneous oscillations in MAP and $S_{ct}O_2$ were found in neonates with HIE during hypothermic therapy; both appeared to be related to worse clinical outcomes. These findings support the feasibility of using this method to assess cerebral autoregulation in neonates with HIE as well as its potential prognostic values for short- and long-term clinical outcome measures in these patients.

Acknowledgments

This work was supported by National Institutes of Health (NIH) funding from NICHD (5K23HD069521-03).

Appendix A. Supplementary data

Supplementary data to this article can be found online at http://dx.doi.org/10.1016/j.nicl.2016.01.020.

References

Aaslid, R., Markwalder, T.M., Nornes, H., 1982. Noninvasive transcranial Doppler ultrasound recording of flow velocity in basal cerebral arteries. J. Neurosurg. 57, 769–774.
Ancora, G., Maranella, E., Grandi, S., Sbravati, F., Coccolini, E., Savini, S., Faldella, G., 2013. Early predictors of short term neurodevelopmental outcome in asphyxiated cooled infants. A combined brain amplitude integrated electroencephalography and near infrared spectroscopy study. Brain Dev. 35, 26–31.
Brady, K.M., Lee, J.K., Kibler, K.K., Smielewski, P., Czosnyka, M., Easley, R.B., Koehler, R.C., Shaffner, D.H., 2007. Continuous time-domain analysis of cerebrovascular autoregulation using near-infrared spectroscopy. Stroke 38, 2818–2825.
Brady, K.M., Lee, J.K., Kibler, K.K., Easley, R.B., Koehler, R.C., Shaffner, D.H., 2008. Continuous measurement of autoregulation by spontaneous fluctuations in cerebral perfusion pressure: comparison of 3 methods. Stroke 39, 2531–2537.
Bryce, J., Boschi-Pinto, C., Shibuya, K., Black, R.E., 2005. WHO estimates of the causes of death in children. Lancet 365, 1147–1152.
Caicedo, A., De Smet, D., Naulaers, G., Ameye, L., Vanderhaegen, J., Lemmers, P., Van Bel, F., Van Huffel, S., 2011a. Cerebral tissue oxygenation and regional oxygen saturation can be used to study cerebral autoregulation in prematurely born infants. Pediatr. Res. 69, 548–553.
Caicedo, A., De Smet, D., Vanderhaegen, J., Naulaers, G., Wolf, M., Lemmers, P., Van Bel, F., Ameye, L., Van Huffel, S., 2011b. Impaired cerebral autoregulation using near-infrared spectroscopy and its relation to clinical outcomes in premature infants. Adv. Exp. Med. Biol. 701, 233–239.
Chalak, L.F., Dupont, T.L., Sanchez, P.J., Lucke, A., Heyne, R.J., Morriss, M.C., Rollins, N.K., 2014a. Neurodevelopmental outcomes after hypothermia therapy in the era of Bayley-III. J. Perinatol.
Chalak, L.F., DuPont, T.L., Sanchez, P.J., Lucke, A., Heyne, R.J., Morriss, M.C., Rollins, N.K., 2014b. Neurodevelopmental outcomes after hypothermia therapy in the era of Bayley-III. J. Perinatol. 34, 629–633.
Chalak, L.F., Tarumi, T., Zhang, R., 2014c. The "neurovascular unit approach" to evaluate mechanisms of dysfunctional autoregulation in asphyxiated newborns in the era of hypothermia therapy. Early Hum. Dev. 90, 687–694.
Cristianini, N., Shawe-Taylor, J., 2000. An Introduction to Support Vector Machines and Other Kernel-based Learning Methods. Cambridge University Press, Cambridge; New York.
Derosiere, G., Dalhoumi, S., Perrey, S., Dray, G., Ward, T., 2014. Towards a near infrared spectroscopy-based estimation of operator attentional state. PLoS One 9, e92045.
Durduran, T., Yodh, A.G., 2014. Diffuse correlation spectroscopy for non-invasive, microvascular cerebral blood flow measurement. NeuroImage 85 (Pt 1), 51–63.
Efron, B., Tibshirani, R., 1993. An Introduction to the Bootstrap. Chapman & Hall, New York.
Georgakoudi, I., Jacobson, B.C., Van Dam, J., Backman, V., Wallace, M.B., Muller, M.G., Zhang, Q., Badizadegan, K., Sun, D., Thomas, G.A., Perelman, L.T., Feld, M.S., 2001. Fluorescence, reflectance, and light-scattering spectroscopy for evaluating dysplasia in patients with Barrett's esophagus. Gastroenterology 120, 1620–1629.
Gilmore, M.M., Stone, B.S., Shepard, J.A., Czosnyka, M., Easley, R.B., Brady, K.M., 2011. Relationship between cerebrovascular dysautoregulation and arterial blood pressure in the premature infant. J. Perinatol. 31, 722–729.
Govindan, R.B., Massaro, A.N., Andescavage, N.N., Chang, T., du Plessis, A., 2014. Cerebral pressure passivity in newborns with encephalopathy undergoing therapeutic hypothermia. Front. Hum. Neurosci. 8, 266.
Greisen, G., 2006. Is near-infrared spectroscopy living up to its promises? Semin. Fetal Neonatal Med. 11, 498–502.
Greisen, G., 2009. To autoregulate or not to autoregulate—that is no longer the question. Semin. Pediatr. Neurol. 16, 207–215.
Grinsted, A., Moore, J.C., Jevrejeva, S., 2004. Application of the cross wavelet transform and wavelet coherence to geophysical time series. Nonlinear Process. Geophys. 11, 561–566.
Hahn, G.H., Heiring, C., Pryds, O., Greisen, G., 2011. Applicability of near-infrared spectroscopy to measure cerebral autoregulation noninvasively in neonates: a validation study in piglets. Pediatr. Res. 70, 166–170.
Higgins, R.D., Raju, T., Edwards, A.D., Azzopardi, D.V., Bose, C.L., Clark, R.H., Ferriero, D.M., Guillet, R., Gunn, A.J., Hagberg, H., Hirtz, D., Inder, T.E., Jacobs, S.E., Jenkins, D., Juul, S., Laptook, A.R., Lucey, J.F., Maze, M., Palmer, C., Papile, L., Pfister, R.H., Robertson, N.J., Rutherford, M., Shankaran, S., Silverstein, F.S., Soll, R.F., Thoresen, M., Walsh, W.F., 2011. Hypothermia and other treatment options for neonatal encephalopathy: an executive summary of the Eunice Kennedy Shriver NICHD workshop. J. Pediatr. 159 (5), 851–858.e1.
Hjorth, J.S.U., 1994. Computer Intensive Statistical Methods: Validation Model Selection and Bootstrap. Chapman & Hall, London; New York.
Laptook, A.R., 2009. Use of therapeutic hypothermia for term infants with hypoxic–ischemic encephalopathy. Pediatr. Clin. N. Am. 56, 601–616 (Table of Contents).
Laptook, A.R., Corbett, R.J., Burns, D.K., Sterett, R., 1999. A limited interval of delayed modest hypothermia for ischemic brain resuscitation is not beneficial in neonatal swine. Pediatr. Res. 46, 383–389.
Laptook, A.R., Shalak, L., Corbett, R.J., 2001. Differences in brain temperature and cerebral blood flow during selective head versus whole-body cooling. Pediatrics 108, 1103–1110.
Latka, M., Turalska, M., Glaubic-Latka, M., Kolodziej, W., Latka, D., West, B.J., 2005. Phase dynamics in cerebral autoregulation. Am. J. Physiol. Heart Circ. Physiol. 289, H2272–H2279.
Lee, J.K., Brady, K.M., Mytar, J.O., Kibler, K.K., Carter, E.L., Hirsch, K.G., Hogue, C.W., Easley, R.B., Jordan, L.C., Smielewski, P., Czosnyka, M., Shaffner, D.H., Koehler, R.C., 2011. Cerebral blood flow and cerebrovascular autoregulation in a swine model of pediatric cardiac arrest and hypothermia. Crit. Care Med. 39, 2337–2345.
Lee, J.K., Yang, Z.J., Wang, B., Larson, A.C., Jamrogowicz, J.L., Kulikowicz, E., Kibler, K.K., Mytar, J.O., Carter, E.L., Burman, H.T., Brady, K.M., Smielewski, P., Czosnyka, M., Koehler, R.C., Shaffner, D.H., 2012. Noninvasive autoregulation monitoring in a swine model of pediatric cardiac arrest. Anesth. Analg. 114, 825–836.
Lemmers, P.M., Zwanenburg, R.J., Benders, M.J., de Vries, L.S., Groenendaal, F., van Bel, F., Toet, M.C., 2013. Cerebral oxygenation and brain activity after perinatal asphyxia: does hypothermia change their prognostic value? Pediatr. Res. 74, 180–185.
Levene, M.L., Kornberg, J., Williams, T.H., 1985. The incidence and severity of post-asphyxial encephalopathy in full-term infants. Early Hum. Dev. 11, 21–26.
Liu, X., Czosnyka, M., Donnelly, J., Budohoski, K.P., Varsos, G.V., Nasr, N., Brady, K.M., Reinhard, M., Hutchinson, P.J., Smielewski, P., 2015. Comparison of frequency and time domain methods of assessment of cerebral autoregulation in traumatic brain injury. J. Cereb. Blood Flow Metab. 35, 248–256.
Mallat, S.G., 1999. A Wavelet Tour of Signal Processing. Academic Press, San Diego.
Maraun, D., Kurths, J., 2004. Cross wavelet analysis: significance testing and pitfalls. Nonlinear Process. Geophys. 11, 505–514.
Meek, J.H., Elwell, C.E., McCormick, D.C., Edwards, A.D., Townsend, J.P., Stewart, A.L., Wyatt, J.S., 1999. Abnormal cerebral haemodynamics in perinatally asphyxiated neonates related to outcome. Arch. Dis. Child. Fetal Neonatal Ed. 81, F110–F115.
Panerai, R.B., 1998. Assessment of cerebral pressure autoregulation in humans—a review of measurement methods. Physiol. Meas. 19, 305–338.
Panerai, R.B., 2014. Nonstationarity of dynamic cerebral autoregulation. Med. Eng. Phys. 36, 576–584.
Pryds, O., Greisen, G., Lou, H., Friis-Hansen, B., 1990. Vasoparalysis associated with brain damage in asphyxiated term infants. J. Pediatr. 117, 119–125.
Roche-Labarbe, N., Carp, S.A., Surova, A., Patel, M., Boas, D.A., Grant, P.E., Franceschini, M.A., 2010. Noninvasive optical measures of CBV, StO(2), CBF index, and rCMRO (2) in human premature neonates' brains in the first six weeks of life. Hum. Brain Mapp. 31, 341–352.
Rollins, N., Booth, T., Morriss, M.C., Sanchez, P., Heyne, R., Chalak, L., 2014. Predictive value of neonatal MRI showing no or minor degrees of brain injury after hypothermia. Pediatr. Neurol. 50, 447–451.
Rowley, A.B., Payne, S.J., Tachtsidis, I., Ebden, M.J., Whiteley, J.P., Gavaghan, D.J., Tarassenko, L., Smith, M., Elwell, C.E., Delpy, D.T., 2007. Synchronization between arterial blood pressure and cerebral oxyhaemoglobin concentration investigated by wavelet cross-correlation. Physiol. Meas. 28, 161–173.
Sarnat, H.B., Sarnat, M.S., 1976. Neonatal encephalopathy following fetal distress. A clinical and electroencephalographic study. Arch. Neurol. 33, 696–705.
Shalak, L., Perlman, J.M., 2004. Hypoxic–ischemic brain injury in the term infant-current concepts. Early Hum. Dev. 80, 125–141.
Shankaran, S., Laptook, A.R., Ehrenkranz, R.A., Tyson, J.E., McDonald, S.A., Donovan, E.F., Fanaroff, A.A., Poole, W.K., Wright, L.L., Higgins, R.D., Finer, N.N., Carlo, W.A., Duara, S., Oh, W., Cotten, C.M., Stevenson, D.K., Stoll, B.J., Lemons, J.A., Guillet, R., Jobe, A.H., National Institute of Child H, Human Development Neonatal Research N, 2005. Whole-body hypothermia for neonates with hypoxic–ischemic encephalopathy. N. Engl. J. Med. 353, 1574–1584.
Shao, J., 1993. Linear-model selection by cross-validation. J. Am. Stat. Assoc. 88, 486–494.
Soul, J.S., Hammer, P.E., Tsuji, M., Saul, J.P., Bassan, H., Limperopoulos, C., Disalvo, D.N., Moore, M., Akins, P., Ringer, S., Volpe, J.J., Trachtenberg, F., du Plessis, A.J., 2007. Fluctuating pressure-passivity is common in the cerebral circulation of sick premature infants. Pediatr. Res. 61, 467–473.
Tian, F., Sharma, V., Kozel, F.A., Liu, H., 2009. Functional near-infrared spectroscopy to investigate hemodynamic responses to deception in the prefrontal cortex. Brain Res. 1303, 120–130.
Toet, M.C., Lemmers, P.M., van Schelven, L.J., van Bel, F., 2006. Cerebral oxygenation and electrical activity after birth asphyxia: their relation to outcome. Pediatrics 117, 333–339.
Torrence, C., Compo, G.P., 1998. A practical guide to wavelet analysis. B. Am. Meteorol. Soc. 79, 61–78.

Torrence, C., Webster, P.J., 1999. Interdecadal changes in the ENSO-monsoon system. J. Clim. 12, 2679–2690.
Tsuji, M., duPlessis, A., Taylor, G., Crocker, R., Volpe, J.J., 1998. Near infrared spectroscopy detects cerebral ischemia during hypotension in piglets. Pediatr. Res. 44, 591–595.
Tsuji, M., Saul, J.P., du Plessis, A., Eichenwald, E., Sobh, J., Crocker, R., Volpe, J.J., 2000. Cerebral intravascular oxygenation correlates with mean arterial pressure in critically ill premature infants. Pediatrics 106, 625–632.
van Bel, F., Lemmers, P., Naulaers, G., 2008. Monitoring neonatal regional cerebral oxygen saturation in clinical practice: value and pitfalls. Neonatology 94, 237–244.
Volpe, J.J., 1981. Neurology of the newborn. Major. Probl. Clin. Pediatr. 22, 1–648.
Volynskaya, Z., Haka, A.S., Bechtel, K.L., Fitzmaurice, M., Shenk, R., Wang, N., Nazemi, J., Dasari, R.R., Feld, M.S., 2008. Diagnosing breast cancer using diffuse reflectance spectroscopy and intrinsic fluorescence spectroscopy. J. Biomed. Opt. 13, 024012.
Welch, P.D., 1967. Use of fast Fourier transform for estimation of power spectra — a method based on time averaging over short modified periodograms. IEEE T Acoust Speech Au 15, 70–73.
Wintermark, P., Hansen, A., Warfield, S.K., Dukhovny, D., Soul, J.S., 2014. Near-infrared spectroscopy versus magnetic resonance imaging to study brain perfusion in newborns with hypoxic–ischemic encephalopathy treated with hypothermia. NeuroImage 85 (Pt 1), 287–293.
Wong, F.Y., Silas, R., Hew, S., Samarasinghe, T., Walker, A.M., 2012. Cerebral oxygenation is highly sensitive to blood pressure variability in sick preterm infants. PLoS One 7, e43165.
Zhang, R., Zuckerman, J.H., Giller, C.A., Levine, B.D., 1998. Transfer function analysis of dynamic cerebral autoregulation in humans. Am. J. Phys. 274, H233–H241.
Zhang, R., Zuckerman, J.H., Iwasaki, K., Wilson, T.E., Crandall, C.G., Levine, B.D., 2002. Autonomic neural control of dynamic cerebral autoregulation in humans. Circulation 106, 1814–1820.
Zonta, M., Angulo, M.C., Gobbo, S., Rosengarten, B., Hossmann, K.A., Pozzan, T., Carmignoto, G., 2003. Neuron-to-astrocyte signaling is central to the dynamic control of brain microcirculation. Nat. Neurosci. 6, 43–50.